Contents list available at CBIORE journal website
International Journal of Renewable Energy Development
Journal homepage: https://ijred.cbiore.id

Research Article

Effect of single-layer graphene incorporation on TiO_2 photoanodes for enhanced photovoltaic performance of chlorophyll-based dye-sensitized solar cells

Uzfi Helmi Zamzami[a*], Prihanto Trihutomo[b], Aminnudin[b], Tuan Amran Tuan Abdullah[c]

[a] *Master Program of Mechanical Engineering, Faculty of Engineering, State University of Malang, Jl. Semarang 5, Malang 65145, Indonesia*
[b] *Department of Mechanical Engineering, State University of Malang, Jl. Semarang 5, Malang 65145, Indonesia*
[c] *Department of Chemical Engineering, Faculty of Chemical & Energy Engineering, Universiti Teknologi Malaysia, Skudal, Johor 81310, Malaysia*

Abstract. The increasing demand for renewable energy technologies has encouraged extensive research on dye-sensitized solar cells (DSSCs) utilizing environmentally friendly and sustainable conductive materials. This study aims to synthesize and characterize TiO_2/single-layer graphene composites as photoanodes to improve electron transport and photovoltaic performance in chlorophyll-based DSSCs. TiO_2/single-layer graphene composites were prepared with graphene concentrations of 0.5%, 1.0%, and 1.5% v/v, while pure TiO_2 was used as the control sample. The synthesized composites were deposited onto FTO substrates as photoanode films, and their structural, morphological, chemical, and optical properties were analyzed using XRD, SEM, FTIR, and UV–Vis spectroscopy. The photovoltaic performance of the fabricated DSSCs was evaluated through current–voltage (I–V) measurements. The results demonstrate that incorporation of single-layer graphene significantly improves crystallinity, surface homogeneity, and interfacial interaction between TiO_2 and graphene, as confirmed by the formation of Ti–O–C bonding. UV–Vis analysis revealed enhanced visible-light absorption, a redshift in the absorption edge, and reduced optical band gap energy after graphene incorporation, indicating improved light-harvesting capability. Among all investigated compositions, the TiO_2/single-layer graphene photoanode containing 1.0% v/v graphene exhibited the highest photovoltaic performance, achieving a power conversion efficiency of 1.09% with a fill factor of 63.7%. However, excessive graphene incorporation at 1.5% v/v caused particle agglomeration and reduced film uniformity, which negatively affected DSSC performance. Overall, moderate incorporation of single-layer graphene effectively enhanced conductivity, charge transport, and photovoltaic properties, highlighting its strong potential as an environmentally friendly conductive material for sustainable chlorophyll-based DSSC applications.

Keywords: TiO_2/single-layer graphene; Dye-sensitized solar cells (DSSCs); Chlorophyll dye; Photoanode; Photovoltaic performance

Received: 4th Feb 2026; Revised: 16th May 2026; Accepted: 29th June 2026; Available online: 20th July 2026

1. Introduction

In Indonesia, the development of renewable energy technologies has become increasingly important due to the country's abundant solar energy resources and the increasing demand for sustainable electricity generation (Lana *et al.,* 2024). Among various photovoltaic technologies, Dye-Sensitized Solar Cells (DSSCs) have attracted considerable attention because of their low production cost, simple fabrication process, transparency, and stable performance under low-light conditions (Bandara, Gunathilake, Dissanayake, *et al.*, 2024).

Titanium dioxide (TiO_2) has been widely employed as the photoanode material in DSSCs because of its favorable band structure, chemical stability, non-toxicity, and low manufacturing cost (Muhammad *et al.*, 2025). However, despite these advantages, conventional TiO_2-based DSSCs still exhibit relatively low power conversion efficiency due to poor intrinsic electrical conductivity, slow electron transport, and severe electron–hole recombination occurring within the photoanode layer (Yeoh *et al.*, 2023). These limitations significantly reduce charge collection efficiency and hinder the practical application of DSSC technology.

To overcome these drawbacks, numerous studies have investigated conductive carbon-based materials as electron transport enhancers in TiO_2 photoanodes (Muchuweni *et al.*, 2025). Among these materials, single-layer graphene has emerged as one of the most promising conductive additives because of its extraordinary electrical conductivity, ultrahigh electron mobility, excellent transparency, and two-dimensional atomic structure that enables rapid electron transport pathways. Previous studies reported that the incorporation of single-layer graphene into TiO_2 photoanodes could improve interparticle electrical connectivity, accelerate electron extraction from dye molecules, and suppress charge recombination within DSSC systems (Prima *et al.*, 2024).

The presence of single-layer graphene also contributes to the formation of continuous conductive networks that facilitate faster electron diffusion and lower internal resistance (Trihutomo, 2024). Consequently, DSSCs incorporating single-layer graphene generally exhibit enhanced photocurrent

* Corresponding author
Email: uzfi.helmi.2305168@students.um.ac.id (U.H.Zamzami)

response and improved photovoltaic performance compared with pristine TiO_2 systems (Trihutomo *et al.*, 2022).

Nevertheless, despite the reported advantages of single-layer graphene, several critical limitations remain unresolved. Most previous investigations primarily focused on DSSCs utilizing synthetic ruthenium-based dyes and commercially synthesized graphene materials, while studies involving natural chlorophyll dyes are still relatively limited (Bandara, Gunathilake, Gamachchi, *et al.*, 2024). Natural dyes possess several advantages, including biodegradability, environmental friendliness, low toxicity, and abundant availability from biomass resources. However, chlorophyll-based DSSCs commonly suffer from weak electron injection capability, narrow light absorption ranges, and poor photostability, which intensify charge recombination and reduce overall device efficiency (Atilgan & Yildiz, 2022).

In addition, although single-layer graphene has been widely reported to enhance conductivity, the relationship between graphene concentration, charge transport behavior, and recombination suppression in chlorophyll-based DSSCs has not yet been comprehensively clarified (Prakash & Janarthanan, 2023). Excessive incorporation of single-layer graphene may also induce agglomeration, reduce light penetration, and block dye adsorption sites on TiO_2 surfaces, ultimately limiting photovoltaic performance. These unresolved issues indicate that optimizing the concentration and interfacial interaction of single-layer graphene within TiO_2 photoanodes remains a significant challenge (Chaudhari *et al.*, 2024).

Therefore, this study focuses on the fabrication and characterization of single-layer graphene-incorporated TiO_2 photoanodes for chlorophyll-based Dye-Sensitized Solar Cells. The present work specifically investigates the influence of single-layer graphene concentration on the structural, morphological, optical, and photovoltaic properties of TiO_2 photoanodes (Znidi *et al.*, 2024). Particular emphasis is placed on understanding the role of single-layer graphene in improving electrical conductivity, facilitating electron transport, and suppressing charge recombination within chlorophyll-based DSSC systems. To comprehensively evaluate the fabricated composites, XRD, SEM, FTIR, UV–Vis spectroscopy, and photovoltaic performance measurements were systematically conducted. The findings of this study are expected to provide important insights into the optimization of single-layer graphene concentration for developing low-cost, environmentally friendly, and high-efficiency chlorophyll-based DSSCs (Teja *et al.*, 2023).

2. Material and Methods

2.1 Materials

The materials used were single-layer graphene (thickness ~0.8 nm, diameter 0.5–5 μm, purity 99%, XF-NANO, China), titanium dioxide (TiO_2, anatase, ≥99%, Sigma-Aldrich, Germany), fluorine-doped tin oxide (FTO) glass (resistivity 15 Ω/sq, Pilkington, UK), ethanol 96% (Merck, Germany), nitric acid (HNO_3, Merck, Germany), acetic acid (CH_3COOH, Emsure, Germany), acetone (C_3H_6O, Merck, Germany), potassium iodide (KI, Sigma-Aldrich, Germany), and iodine (I_2, Sigma-Aldrich, Germany). The dye used was chlorophyll extracted from fresh leaves. All materials were used without further purification.

2.2 Methods

2.2.1 TiO_2–Graphene Fabrication

TiO_2–graphene was synthesized following the procedure reported in a previous study (Kavitha *et al.*, 2024). Graphene dispersions with volume fractions of 0.5, 1.0, and 1.5% v/v were prepared in 50 mL ethanol and subsequently homogenized using magnetic stirring for 60 minutes. TiO_2 powder was progressively incorporated into the graphene suspension, and the mixture was maintained under constant stirring for 2 hours to promote homogeneous dispersion. The obtained mixture was evaporated at 80–100 °C on a hot plate until a paste was formed. The prepared paste underwent oven drying at 80 °C for 1–2 hours to generate a solid TiO_2–graphene composite. The dried product was finely ground and stored for use as a photoanode material in the DSSC assembly, as shown in Figure 1.

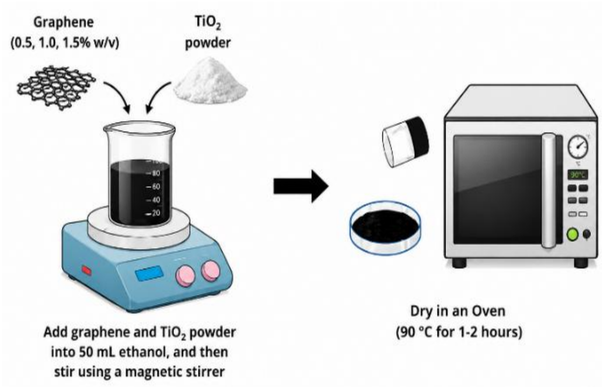

Fig 1. Illustration of TiO_2–graphene Composite Fabrication

2.2.2 Photoanode Layer Fabrication

The fabrication of TiO_2–graphene photoanode films was carried out through several sequential processes, as illustrated in Figure 2. The preparation commenced with the addition of nitric acid (HNO_3) to the TiO_2–graphene paste, followed by magnetic stirring for 30 minutes to promote homogeneous dispersion. The paste was spread onto conductive FTO glass substrates via the doctor blade method, producing a thin, evenly coated film (Shaikh *et al.*, 2024). Drying of the coated films was performed at 80–100 °C for 2 hours to ensure solvent removal. The electrodes were subsequently immersed in chlorophyll dye for 4 hours at room temperature in darkness to facilitate efficient adsorption onto the TiO_2–graphene surface. After dye immersion, the films were removed, air-dried at room temperature, and mildly heated at 50 °C for 30 minutes to enhance dye anchoring and interfacial stability with the TiO_2–graphene photoanode, thereby improving light absorption and charge transfer within the DSSC system.

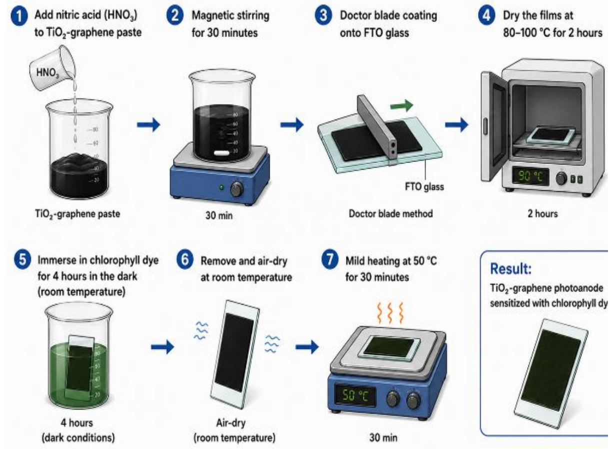

Fig 2. Illustration of TiO_2–graphene photoanode layer fabrication process.

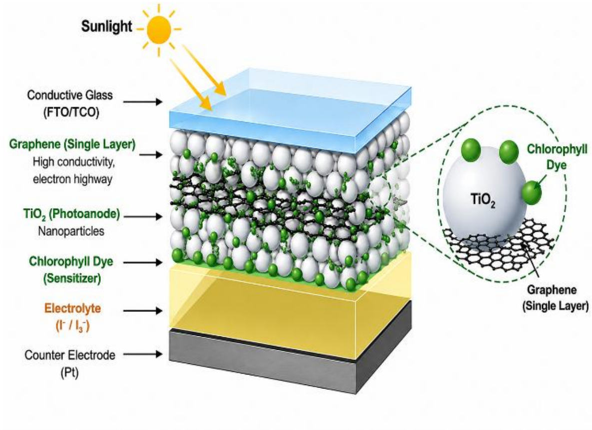

Fig 3. Schematic fabrication process of TiO_2/single-layer graphene photoanodes for chlorophyll-based dye-sensitized solar cells

2.2.3 DSSC Assembly Process

The DSSC device was assembled through a systematic and sequential fabrication procedure, as illustrated in Fig. 3. The TiO_2/single-layer graphene photoanode sensitized with chlorophyll dye was positioned face-to-face with a platinum (Pt)-coated counter electrode deposited on conductive FTO glass (Rahman *et al.*, 2023). Prior to sensitization, chlorophyll dye was extracted from fresh spinach leaves using ethanol as the extraction solvent. The extraction process was performed at room temperature under dark conditions to minimize chlorophyll degradation caused by thermal and photooxidative effects (Prakash & Janarthanan, 2023).

The spinach leaves were washed thoroughly, ground into fine particles, and immersed in ethanol solution under continuous stirring to dissolve chlorophyll pigments effectively. The resulting extract was filtered to remove solid residues and obtain a homogeneous chlorophyll solution suitable for DSSC sensitization (Alamu *et a*l., 2024). The prepared dye solution was subsequently stored in a sealed dark container at low temperature to maintain pigment stability before use.

The fabricated TiO_2/single-layer graphene photoanodes were immersed in the chlorophyll dye solution for several hours to promote effective adsorption of chlorophyll molecules onto the TiO_2/single-layer graphene surface (Igman *et al.*, 2021). The incorporation of single-layer graphene within the TiO_2 matrix provided conductive pathways that facilitated electron transport and improved interfacial interaction between TiO_2 nanoparticles and chlorophyll dye molecules, as schematically shown in Fig. 3. After sensitization, the photoanode and Pt counter electrode were assembled using an adhesive spacer film that simultaneously functioned as a separator and sealant to preserve the structural stability of the DSSC device (Erdogdu *et al.*, 2024).

Subsequently, a potassium iodide/triiodide (KI/I_3^-)-based electrolyte was carefully injected into the inter-electrode space through a filling hole until the active area was completely saturated. The assembled DSSC cell was then tightly clamped using binder clips to ensure firm substrate contact and to prevent electrolyte leakage during operation (Richhariya, Kumar, Shukla, Shukla, & Meikap, 2023). Finally, the completed DSSC device was stored at room temperature prior to photovoltaic characterization and performance evaluation (Hosseinnezhad *et al.*, 2024).

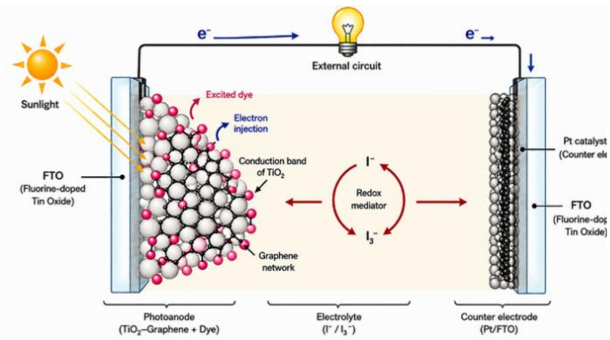

Fig 4. Schematic illustration of the dye-sensitized solar cells (DSSC)

2.2.4 DSSC Fabrication

The fabrication structure and electron transfer mechanism of the TiO_2/single-layer graphene-based Dye-Sensitized Solar Cell (DSSC) are schematically illustrated in Fig. 4. The assembled DSSC device consisted of a TiO_2/single-layer graphene photoanode deposited on fluorine-doped tin oxide (FTO) conductive glass, an iodide/triiodide (I^-/I_3^-)-based electrolyte, and a platinum (Pt)-coated counter electrode. The TiO_2/single-layer graphene photoanode previously sensitized with chlorophyll dye was positioned face-to-face with the Pt counter electrode and separated using an adhesive spacer layer to maintain a stable inter-electrode distance and prevent electrolyte leakage (Prima *et al.*, 2024).

Subsequently, the electrolyte solution containing the iodide/triiodide redox mediator was carefully injected into the inter-electrode gap until the active region was completely filled. The assembled DSSC device was then tightly clamped to ensure good interfacial contact between both electrodes before photovoltaic characterization.

Under sunlight irradiation, chlorophyll dye molecules adsorbed on the TiO_2/single-layer graphene surface absorbed photon energy and became photoexcited (Amollo, 2024). The absorbed light promoted electrons from the ground state of the dye molecules into an excited electronic state. These excited electrons were subsequently injected into the conduction band of TiO_2 and rapidly transported through the incorporated single-layer graphene network toward the conductive FTO substrate and external circuit (Ding *et al.*, 2023).

The presence of single-layer graphene provided highly conductive electron transport pathways due to its exceptional electrical conductivity and ultrahigh electron mobility (Alhaji Abubakar *et al.*, 2025). This conductive network accelerated electron diffusion and significantly suppressed electron recombination within the TiO_2 photoanode layer, thereby improving charge collection efficiency in the DSSC system. After electron injection, the chlorophyll dye molecules became oxidized (Dye^+) because of electron loss (Mahalingam *et al.*, 2023a). To restore the dye molecules into their original stable state, regeneration occurred through the iodide/triiodide (I^-/I_3^-) electrolyte system.

Ion iodide (I^-) in the electrolyte donated electrons to the oxidized dye molecules, allowing the dye to return to its ground state and enabling continuous light absorption during DSSC operation. During this regeneration process, iodide ions were oxidized into triiodide ions (I_3^-) through the redox reaction mechanism. The regeneration and oxidation reactions can be represented as follows:

$$Dye^+ + 2I^- \rightarrow \; Dye + I_2 + e^-$$
$$I_2 + I^- \rightarrow I_3^-$$

The generated triiodide ions (I_3^-) subsequently diffused through the electrolyte toward the platinum-coated counter electrode

(Agrawal *et al.*, 2022). At the Pt electrode surface, electrons returning from the external circuit reduced triiodide ions back into iodide ions, thereby completing the redox cycle and maintaining continuous charge transfer within the DSSC device. Platinum acted as an efficient electrocatalyst that accelerated the reduction reaction and enhanced the electrochemical stability of the DSSC system (Konwar *et al.*, 2023). The reduction process occurring at the counter electrode can be expressed as follows:

$$I_3^- + 2e^- \rightarrow 3I^-$$

The regenerated iodide ions then migrated back toward the photoanode region to participate again in dye regeneration, creating a continuous cyclic electron transfer process during DSSC operation (Siddiqui *et al.*, 2024).

Overall, the integration of TiO_2, single-layer graphene, chlorophyll dye, and the iodide/triiodide electrolyte system established an efficient charge transport mechanism capable of converting solar energy into electrical energy. The incorporation of single-layer graphene not only enhanced electrical conductivity and electron transport efficiency but also reduced recombination losses and improved interfacial charge transfer between TiO_2 nanoparticles and chlorophyll dye molecules, thereby contributing to enhanced DSSC photovoltaic performance (Chou, Chen, *et al.*, 2023).

3. Results and Discussion

3.1 Characterization of TiO_2–graphene

3.1.1 SEM-EDX

SEM–EDX analysis was conducted to investigate the surface morphology and elemental composition of the TiO_2/single-layer graphene photoanode composites. Figure 5 presents the SEM images of pristine TiO_2 and TiO_2/single-layer graphene composites with different graphene concentrations, all of which exhibit irregular nanoparticle morphologies with varying degrees of agglomeration, porosity, and particle distribution. In the pristine TiO_2 sample (Figure 5a) (Tiwari *et al.*, 2024), the photoanode surface displayed a relatively compact and dense morphology with closely packed nanoparticles distributed throughout the surface. Although the particles appeared relatively uniform in size, the structure showed limited pore formation and restricted interparticle spacing. This compact morphology may reduce electrolyte penetration and limit the effective surface area available for chlorophyll dye adsorption (Richhariya, Kumar, Shukla, Shukla, & Meikap, 2023).

Following the incorporation of 0.5% v/v single-layer graphene (Figure 5b), the TiO_2 surface became rougher and more porous, with nanoparticles appearing more loosely distributed compared to the pristine TiO_2 sample. The addition of graphene reduced excessive particle packing and promoted the formation of interparticle voids across the photoanode layer. This morphological transformation is expected to improve electrolyte diffusion and facilitate electron transport pathways within the DSSC structure. Similar observations were reported, where graphene incorporation enhanced the porosity and conductivity of TiO_2-based photoanodes by improving nanoparticle dispersion and suppressing aggregation (Chakraborty *et al.*, 2024).

At a graphene concentration of 1.0% v/v (Figure 5c), the composite exhibited the most homogeneous nanoparticle distribution among all samples. The TiO_2 nanoparticles were uniformly dispersed with interconnected porous structures and minimal agglomeration, as indicated by the relatively even surface morphology. The homogeneous distribution suggests that single-layer graphene was effectively integrated within the TiO_2 matrix, forming conductive electron transport networks while maintaining adequate porosity for chlorophyll dye adsorption and electrolyte infiltration (Saadat *et al.*, 2022). The enhanced pore distribution and reduced particle clustering are expected to improve the active surface area and facilitate more efficient electron transport in the DSSC system.

However, increasing the graphene concentration to 1.5% v/v (Figure 5d) resulted in significant particle agglomeration and reduced structural uniformity. Large particle clusters and graphene restacking became clearly visible, producing a denser morphology with lower pore distribution compared to the 1.0% v/v sample.

Excessive graphene loading promoted nanoparticle aggregation due to strong van der Waals interactions between graphene sheets, leading to non-uniform conductive pathways throughout the photoanode structure. This agglomeration behavior may hinder light penetration, reduce chlorophyll dye adsorption sites, and increase charge recombination within the DSSC layer (Vibavakumar *et al.*, 2024). Similar findings were reported by Zheng *et a*l. (2024), who observed that excessive graphene incorporation induced aggregation and reduced electron transport effectiveness in graphene-based photoanodes (Zheng *et al.*, 2024).

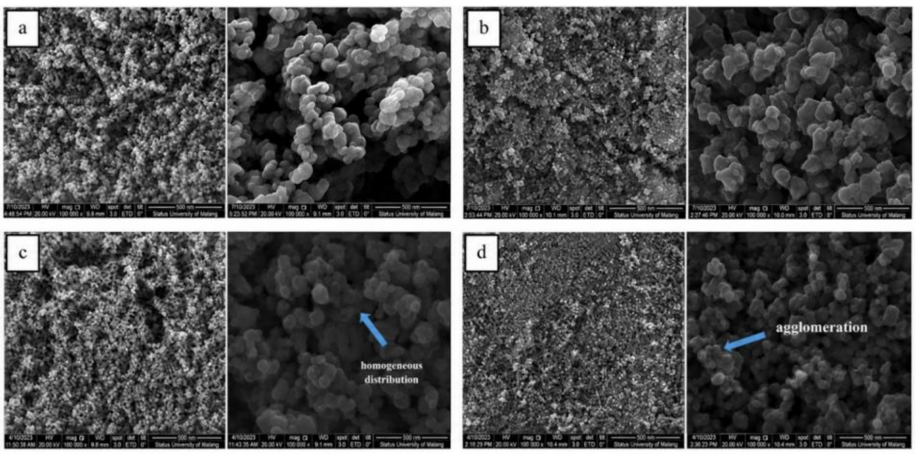

Fig 5. Morphology of: (a) TiO_2 control; TiO_2–graphene composites with (b) 0.5%v/v, (c) 1.0%v/v, and (d) 1.5%v/v graphene concentrations (left: surface morphology; right: cross

Table 1
Weight Percentage of Elements Obtained from EDX Analysis at Different Single-Layer Graphene Concentrations

Element (Weight %)	Sample			
	Pure TiO_2	TiO_2–Graphene 0.5% v/v	TiO_2–Graphene 1 % v/v	TiO_2–Graphene 1.5% v/v
C	-	4.50	10.05	9.68
N	-	-	-	1.61
O	60.58	47.07	27.09	42.79
Si	-	-	0.50	-
Ti	39.42	48.44	62.36	45.92

Table 2
Atomic Percentage of Elements Obtained from EDX Analysis at Different Single-Layer Graphene Concentrations

Element (Atomic %)	Sample			
	Pure TiO_2	TiO_2–Graphene 0.5% v/v	TiO_2–Graphene 1 % v/v	TiO_2–Graphene 1.5% v/v
C	-	8.65	21.73	17.71
N	-	-	-	2.52
O	82.14	67.97	43.98	58.72
Si	-	-	0.47	-
Ti	17.86	23.37	33.83	21.06

The elemental composition of the TiO_2/single-layer graphene composites was further analyzed using EDX, as presented in Tables 2 and 3. The EDX results confirmed that titanium (Ti) and oxygen (O) were the dominant elements in all samples, indicating successful formation of the TiO_2-based photoanode structure. In the pristine TiO_2 sample corresponding to Figure 5a, only Ti and O elements were detected, with concentrations of 39.42 wt.% Ti and 60.58 wt.% O, confirming the absence of graphene within the photoanode layer.

For the 0.5% v/v graphene sample shown in Figure 5b, carbon (C) was detected at 4.50 wt.%, accompanied by 48.44 wt.% Ti and 47.07 wt.% O, confirming the successful incorporation of single-layer graphene into the TiO_2 matrix. Increasing the graphene concentration to 1.0% v/v in Figure 5c significantly increased the carbon content to 10.05 wt.%, while Ti remained dominant at 62.36 wt.%. The high carbon content observed in Figure 5c corresponds well with the homogeneous nanoparticle distribution shown in the SEM image, indicating effective graphene dispersion throughout the TiO_2 structure (Shikh Zahari *et al*., 2023).

In contrast, the 1.5% v/v graphene sample shown in Figure 5d exhibited 9.68 wt.% carbon, 45.92 wt.% Ti, and 42.79 wt.% O, together with visible agglomeration observed in the SEM image. These findings suggest that excessive graphene addition promoted graphene restacking and nanoparticle aggregation, reducing structural uniformity despite the relatively high carbon concentration.

Minor impurity elements, including nitrogen (N) and silicon (Si), were also detected in small amounts. Nitrogen was observed only in Figure 5d at 1.61 wt.%, while silicon was detected in Figure 5c at 0.50 wt.%. These trace elements were likely associated with residual precursor materials, environmental exposure, or substrate-related interference from the FTO glass during EDX analysis (Iman *et al*., 2024). Since the concentrations were relatively low, their presence was considered negligible and unlikely to significantly influence the structural and photovoltaic performance of the TiO_2/single-layer graphene photoanodes.

Overall, the SEM and EDX analyses demonstrate that single-layer graphene concentration strongly influences the morphological characteristics and elemental distribution of the TiO_2 photoanode layer. The incorporation of graphene at an optimal concentration improved nanoparticle homogeneity, pore distribution, and conductive electron transport pathways, whereas excessive graphene loading promoted agglomeration and reduced surface uniformity. These structural and compositional changes are expected to significantly affect dye adsorption capability, electrolyte diffusion, charge transport behavior, and ultimately the photovoltaic performance of the DSSC device.

3.1.2 FTIR

The FTIR spectra presented in Figure 6 reveal significant variations in the vibrational characteristics and functional group distribution of the TiO_2/single-layer graphene composites with different graphene concentrations. Several prominent absorption bands associated with TiO_2 and carbon-based structures were observed, indicating successful incorporation of single-layer graphene into the TiO_2 matrix, as summarized in Table 3. The broad absorption band detected within the range of 3200–3500 cm^{-1} corresponds to O–H stretching vibrations originating from surface hydroxyl groups and adsorbed water molecules on the TiO_2 surface (Erdogdu *et al*., 2024).

The intensity of this band gradually increased with increasing single-layer graphene concentration, suggesting enhanced surface interaction and stronger hydrogen-bonding behavior within the composite structure (Hosseinnezhad *et al*., 2023). The presence of hydroxyl groups is particularly important in DSSC systems because these groups contribute to dye adsorption capability and improve interfacial contact between chlorophyll molecules and the TiO_2 surface. In addition, the slight shift of the O–H peak toward higher wavelengths after graphene incorporation indicates modification of the local chemical environment due to interactions between TiO_2 nanoparticles and the graphene network.

Absorption peaks located in the range of 2800–3000 cm^{-1} are attributed to C–H stretching vibrations associated with residual organic compounds and carbonaceous structures within the composite. These peaks remained observable in all samples, although variations in peak intensity were detected after graphene addition (Chang *et a*l., 2020). The persistence of C–H vibrations indicates that carbon-containing structures from single-layer graphene were successfully retained during the fabrication process. Furthermore, the absorption region

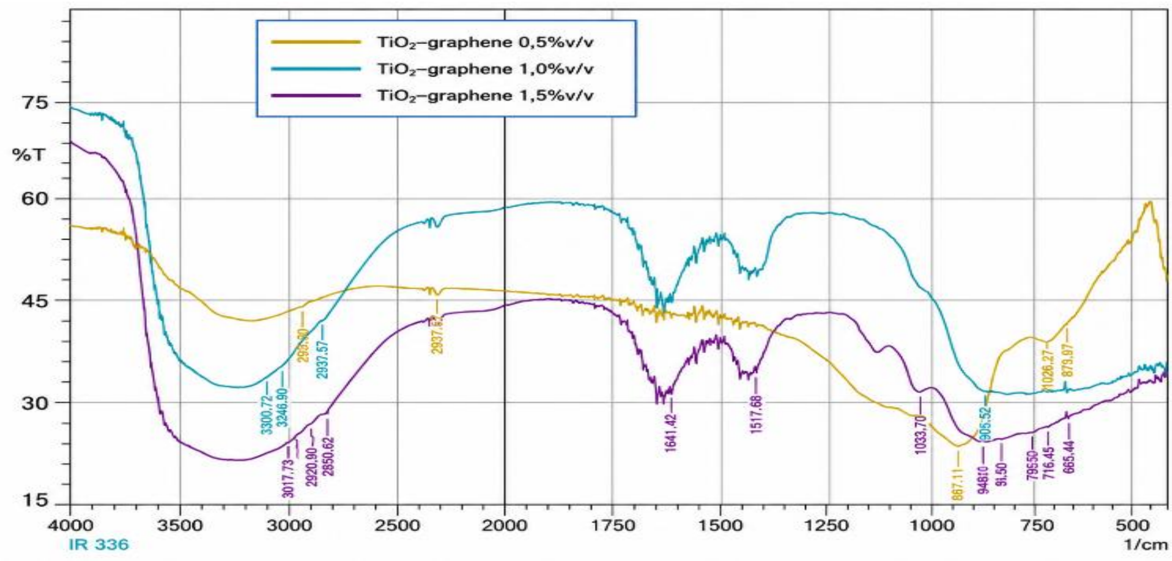

Fig 6. FTIR spectra of TiO_2/single-layer graphene photoanodes at different graphene concentrations in the wavenumber range of 4000–400 cm^{-1}.

between 1500 and 1650 cm^{-1} corresponds to C=C stretching vibrations originating from the sp² carbon network of single-layer graphene.

The intensity and peak area of the C=C band progressively increased from Pure TiO_2 to TiO_2–graphene 1.5% v/v confirming the increasing contribution of graphene within the TiO_2 matrix. This behavior demonstrates the successful formation of conductive carbon pathways that potentially facilitate faster electron transport within the DSSC photoanode. The enhanced C=C peak intensity also indicates improved graphitic characteristics and stronger electronic interactions between TiO_2 and graphene sheets, which are beneficial for suppressing charge recombination during photovoltaic operation.

The absorption bands observed within the range of 1200–1450 cm^{-1} are associated with C=O functional groups and oxygen-containing surface species. Variations in this region indicate changes in surface chemistry after graphene incorporation, particularly involving interfacial interactions between TiO_2 particles and graphene layers. Meanwhile, peaks detected near 1000–1300 cm^{-1} correspond to C–O functional groups, suggesting the presence of residual oxygenated carbon structures that may contribute to enhanced dye anchoring behavior (Torres & De-la-Torre, 2022).

In the lower wavenumber region, absorption peaks around 500–700 cm^{-1} are attributed to Ti–O and Ti–O–Ti lattice vibrations, confirming the preservation of the anatase TiO_2 framework after graphene addition. Slight shifts in these Ti–O-

Table 3
The Effect of Single-Layer Graphene Incorporation on Functional Groups of TiO_2 Composites

Functional Group	Wavelength (cm^{-1})			
	Pure TiO_2	TiO_2–Graphene 0.5% v/v	TiO_2–Graphene 1 % v/v	TiO_2–Graphene 1.5% v/v
O-H	3342	3345	3348	3351
C-H	2921	2918	2915	2912
C=C	1631	1627	1623	1619
C=O	1418	1415	1412	1409
C-O	1118	1112	1109	1105
Ti-O-Ti	671	668	665	662
Ti-O Bond	540	537	534	531

Table 4
The Effect of Single-Layer Graphene Incorporation on Total FTIR Peak Area of TiO_2 Composites

Functional Group	Wavelength (cm^{-1})			
	Pure TiO_2	TiO_2–Graphene 0.5% v/v	TiO_2–Graphene 1 % v/v	TiO_2–Graphene 1.5% v/v
O-H	1.284	1.396	1.512	1.431
C-H	0.412	0.536	0.648	0.593
C=C	0.921	1.284	1.763	1.942
C=O	0.638	0.814	1.032	1.087
C-O	1.432	1.287	1.164	1.058
Ti-O-Ti	2.418	2.305	2.184	2.063
Ti-O Bond	1.865	1.754	1.621	1.503
Total Peak Area	8.970	9.376	9.924	9.677

related peaks indicate possible structural interaction and partial electronic coupling between TiO_2 and single-layer graphene. Based on the total peak area analysis shown in Table 4, the incorporation of graphene generally increased the total functional group intensity (Raveena *et al.*, 2023), particularly at the TiO_2–graphene 1.0% v/v graphene concentration. This increase suggests improved surface activity and stronger interfacial interaction within the composite system. However, excessive graphene loading at TiO_2–graphene 1.5% v/v slightly reduced the total peak area, which may be associated with graphene agglomeration and partial shielding of active TiO_2 surfaces (Tiwari *et al.*, 2024). Overall, the FTIR analysis confirms that single-layer graphene incorporation significantly influences the chemical structure, surface functionality, and interfacial characteristics of the TiO_2 photoanode, which are expected to contribute to enhanced electron transport and improved DSSC photovoltaic performance.

3.1.3 XRD

XRD analysis was performed to investigate the crystal structure and structural evolution of the TiO_2/single-layer graphene photoanodes after graphene incorporation. The diffraction parameters obtained from all samples are summarized in Table 5. All diffraction patterns exhibited a dominant peak located at approximately $2\theta \approx 25°$, corresponding to the (101) crystal plane of anatase TiO_2. The absence of additional diffraction peaks associated with rutile or brookite phases indicates that the incorporation of single-layer graphene did not alter the primary anatase crystal structure of TiO_2. These results demonstrate that the anatase phase remained structurally stable throughout the graphene addition process (Qamar & Erten Ela, 2024).

The pristine TiO_2 sample Pure TiO_2 exhibited a diffraction peak at 25.26° with moderate intensity and the broadest diffraction width (FWHM = 0.62), corresponding to a crystallite size of approximately 14.8 nm. The relatively broad diffraction peak suggests lower crystal ordering and the presence of structural imperfections within the TiO_2 matrix. Such conditions may hinder electron mobility and accelerate electron–hole recombination during DSSC operation, thereby limiting photovoltaic performance (Yan *et a*l., 2025).

Following the addition of TiO_2–graphene 0.5% v/v, the diffraction peak slightly shifted to 25.31° and displayed increased intensity accompanied by a reduced FWHM value of 0.54. The calculated crystallite size increased to approximately 17.0 nm, indicating improved crystal growth and enhanced structural ordering (Ma'arifah *et al.*, 2025). The sharper diffraction profile suggests that single-layer graphene contributed to a more homogeneous TiO_2 crystal distribution while suppressing excessive nanoparticle agglomeration. This improvement is associated with the conductive nature of graphene, which may facilitate better interparticle interaction and electron transport pathways within the photoanode structure (Bhumika *et a*l., 2026).

The TiO_2/single-layer graphene sample containing 1.0% v/v graphene demonstrated the highest crystallinity among all samples, as indicated by the highest diffraction intensity and the lowest FWHM value of 0.48. The crystallite size further increased to approximately 19.2 nm, suggesting the formation of larger and more ordered crystallites. The sharper and more intense diffraction peak indicates enhanced crystal homogeneity and stronger interfacial interaction between TiO_2 and single-layer graphene. This structural improvement is expected to facilitate faster electron transport, reduce charge trapping, and suppress electron–hole recombination within the

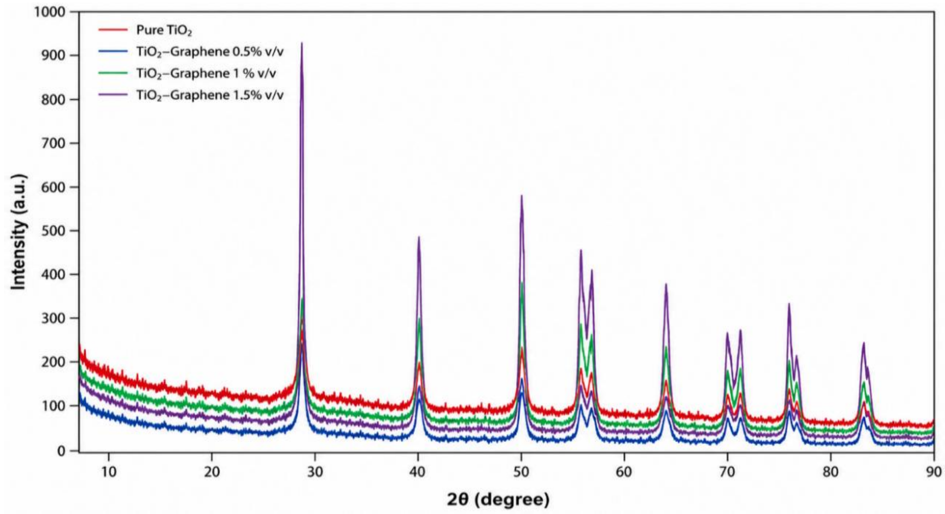

Fig 7. XRD patterns of TiO_2/single-layer graphene photoanodes with different graphene concentrations showing the anatase crystal structure and diffraction peak evolution after graphene incorporation.

Table 5
Structural parameters obtained from XRD analysis of TiO_2/single-layer graphene photoanodes with different graphene concentrations.

Sample	Main Peak (101) 2θ (°)	Relative Intensity	FWHM	Crystallite Size (nm)	Phase
Pure TiO_2	25.26	Moderate	0.62	14.8	Anatase TiO_2
TiO_2–Graphene 0.5% v/v	25.31	High	0.54	17.0	Anatase TiO_2 + graphene
TiO_2–Graphene 1% v/v	25.37	Highest	0.48	19.2	Anatase TiO_2 + graphene
TiO_2–Graphene 1.5% v/v	25.29	Very High	0.59	15.6	Anatase TiO_2 + graphene

DSSC photoanode layer, thereby contributing to improved photovoltaic performance (Irfan *et a*l., 2022).

However, increasing the graphene concentration to 1.5% v/v resulted in a slight broadening of the diffraction peak, with the FWHM increasing to 0.59 and the crystallite size decreasing to approximately 15.6 nm. Although the diffraction intensity remained relatively high, the reduced crystal size and broader peak profile indicate the onset of structural disorder and partial agglomeration within the composite. Excessive graphene loading may promote graphene sheet restacking through van der Waals interactions, which can disrupt the uniform distribution of TiO_2 nanoparticles and reduce structural homogeneity.

Overall, the XRD results demonstrate that moderate incorporation of single-layer graphene significantly improved the structural characteristics of TiO_2 photoanodes by enhancing crystallinity, increasing crystal ordering, and promoting more homogeneous particle distribution (Tiwari *et a*l., 2024). Among all compositions, the 1.0% v/v graphene sample exhibited the most favorable structural properties for DSSC applications. In contrast, excessive graphene incorporation at 1.5% v/v induced partial agglomeration and reduced structural uniformity, which may adversely influence charge transport behavior and photovoltaic efficiency.

3.1.4 UV-VIS

UV–Vis spectroscopy was employed to evaluate the optical absorption characteristics of TiO_2/single-layer graphene photoanodes at different graphene concentrations. The absorption spectra presented in Figure 8 reveal that all samples exhibited strong absorption in the ultraviolet region between 200–350 nm, corresponding to the intrinsic electronic transition of anatase TiO_2. The incorporation of single-layer graphene significantly influenced both the absorption intensity and the absorption edge of the photoanodes (Mandal & Kandregula, 2023).

The pristine TiO_2 photoanode exhibited a maximum absorption peak (λmax) near 295 nm with moderate absorbance intensity and an absorption edge around 385 nm, corresponding to an estimated band gap energy of approximately 3.22 eV. This value is consistent with the characteristic band gap of anatase TiO_2, which primarily absorbs light in the ultraviolet region. However, the relatively wide band gap limits visible-light utilization and reduces photon harvesting efficiency in DSSC applications (Ashfaq *et al*., 2023).

Following the incorporation of 0.5% v/v single-layer graphene, the absorption peak shifted slightly toward a longer wavelength (~300 nm) accompanied by increased absorbance intensity and a broader absorption edge near 395 nm. The estimated band gap decreased to approximately 3.10 eV, indicating that graphene incorporation enhanced visible-light absorption capability. The conductive nature of single-layer graphene likely facilitated electronic interaction between graphene sheets and TiO_2 nanoparticles, thereby narrowing the effective band gap and improving charge transfer behavior (Ramaripa *et al*., 2023).

The TiO_2/single-layer graphene 1.0% v/v sample demonstrated the highest absorption intensity among all photoanodes with λmax observed near 305 nm and an absorption edge extending to approximately 410 nm. The estimated band gap further decreased to around 2.95 eV, suggesting improved electronic interaction and enhanced photon utilization within the composite structure. The reduction in band gap energy indicates that moderate graphene incorporation successfully expanded the optical response of TiO_2 toward the visible-light region, which is highly beneficial for chlorophyll-based DSSC performance (Athanasopoulos & Conradie, 2024).

However, increasing the graphene concentration to 1.5% v/v resulted in a slight decrease in absorbance intensity and a minor increase in band gap energy to approximately 3.02 eV. Although the absorption edge remained broader than that of pure TiO_2, excessive graphene incorporation may have induced graphene agglomeration and partial shielding of active TiO_2 surfaces. Such agglomeration can reduce light penetration and limit effective interaction between TiO_2 and chlorophyll dye molecules, thereby decreasing overall optical performance (Mahalingam *et al*., 2022).

Overall, the UV–Vis results demonstrate that moderate incorporation of single-layer graphene effectively enhanced the optical absorption behavior of TiO_2 photoanodes by increasing absorbance intensity, broadening the absorption edge, and reducing band gap energy. These improvements are expected to facilitate better light harvesting capability, faster electron transport, and reduced charge recombination in chlorophyll-based DSSC systems (Sharma *et al*., 2023).

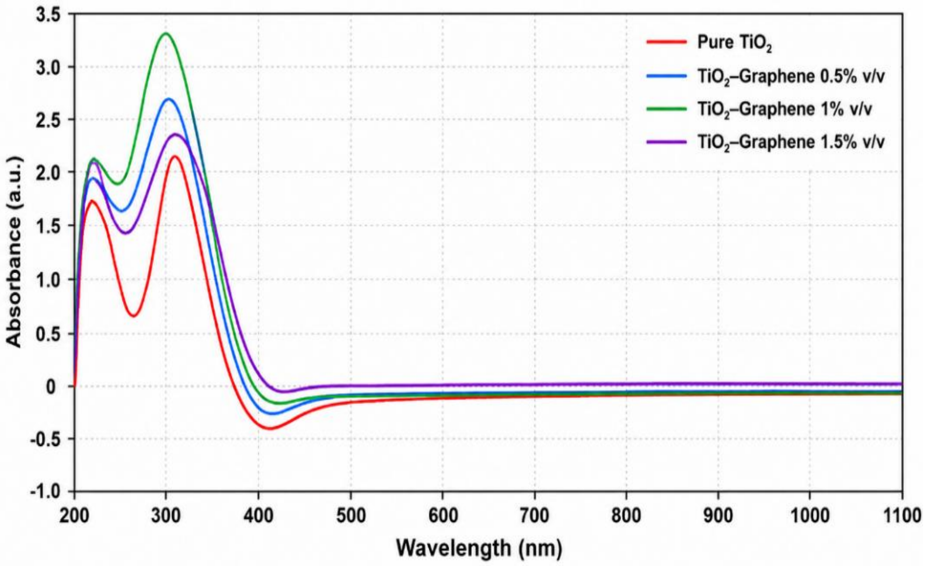

Fig 8. UV–Vis absorption spectra of TiO_2/single-layer graphene photoanodes at different graphene concentrations in the wavelength range of 200–1100 nm.

3.1.5 Power Conversion Efficiency (PCE)

The photovoltaic performance of chlorophyll-based DSSCs fabricated using TiO_2/single-layer graphene photoanodes was evaluated through current–voltage (I–V) characterization under light irradiation, and the obtained parameters are summarized in Table 6. The measured parameters include open-circuit voltage (V_{oc}), short-circuit current density (I_{sc}), maximum power voltage (V_{mp}), maximum power current density (I_{mp}), fill factor (FF), and power conversion efficiency (PCE). The results demonstrate that the incorporation of single-layer graphene significantly influenced the charge transport behavior and photovoltaic performance of the DSSC devices. The pristine TiO_2 photoanode exhibited the lowest photovoltaic performance, with a Voc of 0.52 V, Isc of 0.36 mA/cm², and PCE of 0.82%.

The relatively low efficiency is associated with the intrinsic limitations of pure TiO_2, including low electrical conductivity, slow electron transport kinetics, and rapid electron–hole recombination within the photoanode layer (Muhammad *et a*l., 2025). These results are consistent with the XRD analysis, which showed broader diffraction peaks and lower crystallinity for the pure TiO_2 sample. SEM observations also revealed relatively dense particle aggregation and lower surface homogeneity, which may hinder effective electron mobility and dye adsorption. In addition, UV–Vis analysis demonstrated a relatively wide band gap (~3.22 eV) and limited visible-light absorption capability, reducing the efficiency of photon harvesting within the DSSC system.

Following the incorporation of 0.5% v/v single-layer graphene, the photovoltaic performance improved noticeably, where the Voc increased to 0.54 V and the Isc increased to 0.48 mA/cm², resulting in a PCE of 0.92%. This enhancement indicates that single-layer graphene successfully improved electron transport pathways within the TiO_2 matrix. The conductive graphene network likely facilitated faster electron transfer from the photoexcited chlorophyll dye molecules into the TiO_2 conduction band and subsequently toward the FTO substrate while suppressing charge recombination (Ayaz et al., 2024). This improvement is supported by SEM analysis, which revealed a more porous and homogeneous surface morphology after graphene incorporation. Furthermore, UV–Vis characterization showed enhanced absorbance intensity and reduced band gap energy (~3.10 eV), indicating improved visible-light absorption capability (Maurya *et al.*, 2024).

The highest DSSC performance was obtained for the TiO_2/single-layer graphene 1.0% v/v sample, which achieved a Voc of 0.56 V, Isc of 0.62 mA/cm², FF of 63.7%, and maximum PCE of 1.09%. The enhancement in photovoltaic efficiency strongly correlates with the structural and optical properties observed in the previous characterizations. XRD analysis demonstrated the highest diffraction intensity and the lowest FWHM value, indicating improved crystallinity and more uniform crystallite distribution (Bousrez *et al.*, 2021). SEM observations showed enhanced surface homogeneity and reduced TiO_2 agglomeration, providing a larger active surface area for chlorophyll dye adsorption (Xu *et a*l., 2020). In addition, UV–Vis analysis revealed the strongest absorbance intensity and the lowest estimated band gap (~2.95 eV), indicating broader visible-light absorption and improved photon harvesting capability (Sharma *et a*l., 2023).

These combined structural and optical improvements promoted more efficient electron injection (Mahalingam *et al.*, 2023b), accelerated electron transport, and reduced recombination losses within the DSSC photoanode layer. However, further increasing the graphene concentration to 1.5% v/v resulted in a slight decrease in photovoltaic performance, where the PCE decreased to 0.96%, despite relatively high Voc and Isc values. This reduction is associated with excessive graphene loading, which induced particle agglomeration and reduced film uniformity, as observed in the SEM images. XRD analysis also indicated a slight decrease in crystallinity accompanied by broader diffraction peaks compared with the 1.0% v/v sample.

Excessive graphene incorporation may cause graphene restacking and partial blockage of active TiO_2 surfaces, thereby reducing light penetration and limiting effective dye adsorption (Muchuweni *et a*l., 2022). Consequently, electron transport pathways become less efficient and charge recombination probability increases within the DSSC system. Although the obtained PCE values remain relatively moderate compared with conventional ruthenium-based DSSCs, the incorporation of single-layer graphene successfully enhanced the photovoltaic performance of chlorophyll-based DSSCs (Igman *et al.*, 2021).

The improved efficiency demonstrates the important role of single-layer graphene in facilitating electron transport, broadening light absorption behavior (Amollo, 2024), and suppressing electron recombination within environmentally friendly and low-cost DSSC systems. Overall, the TiO_2/single-layer graphene 1.0% v/v photoanode exhibited the optimum balance between crystallinity, surface morphology, optical absorption, and electrical conductivity, resulting in the highest DSSC efficiency among all investigated samples.

Table 6
Optical Absorption Parameters of TiO_2/Single-Layer Graphene Photoanodes Derived from UV–Vis Analysis.

Sample	λmax (nm)	Absorbance Intensity	Absorption Edge (nm)	Estimated Band Gap (eV)
Pure TiO_2	~ 295	Moderate	~ 385	~ 3.22
TiO_2–Graphene 0.5% v/v	~300	High	~395	~3.10
TiO_2–Graphene 1% v/v	~305	Highest	~410	~2.95
TiO_2–Graphene 1.5% v/v	~302	Moderate-High	~400	~3.02

Table 7
Photovoltaic Parameters of TiO_2/Single-Layer Graphene DSSCs at Different Graphene Concentrations

Sample	V_{oc} (V)	I_{SC} (mA/cm²)	V_{mp} (V)	I_{mp} (mA/cm²)	Fill Factor (%)	PCE(%)
Pure TiO_2	0.52	0.36	0.41	0.27	59.2	0.82
TiO_2–Graphene 0.5% v/v	0.55	0.51	0.45	0.39	62.3	0.92
TiO_2–Graphene 1% v/v	0.58	0.67	0.48	0.52	64.1	1.09
TiO_2–Graphene 1.5% v/v	0.56	0.58	0.46	0.43	61.8	0.96

4. Conclusion

TiO_2/single-layer graphene photoanodes for chlorophyll-based Dye-Sensitized Solar Cells (DSSCs) were successfully fabricated and characterized through structural, morphological, optical, and photovoltaic analyses. The incorporation of single-layer graphene significantly influenced the crystallinity, surface morphology, optical absorption behavior, and photovoltaic performance of the TiO_2 photoanodes. XRD analysis confirmed that all samples retained the anatase TiO_2 crystal phase after graphene incorporation (Richhariya, Kumar, Shukla, Shukla, & Chanakaewsomboon, 2023), while moderate graphene addition improved crystallinity and reduced crystallite size. The TiO_2/single-layer graphene 1.0% v/v sample exhibited the highest diffraction intensity and lowest FWHM value (Ma'arifah *et al.*, 2025), indicating improved crystal homogeneity and enhanced structural ordering.

SEM observations revealed that graphene incorporation modified the surface morphology of the TiO_2 photoanodes by reducing particle agglomeration and increasing surface porosity (Dissanayake et al., 2025). The 1.0% v/v graphene sample showed the most homogeneous particle distribution and improved interparticle connectivity, which are beneficial for electron transport and dye adsorption. However, excessive graphene loading at 1.5% v/v promoted particle agglomeration and reduced surface uniformity (Kouhestanian *et al.*, 2020), potentially hindering charge transport within the DSSC system.

UV–Vis characterization demonstrated that single-layer graphene enhanced the optical absorption capability of the TiO_2 photoanodes. The incorporation of graphene caused a red shift in the absorption edge and reduced the estimated band gap energy from approximately 3.22 eV for pure TiO_2 to 2.95 eV for the 1.0% v/v graphene sample. These optical improvements indicate enhanced visible-light harvesting capability and stronger electronic interaction between TiO_2 and single-layer graphene, which contributed to improved photoresponse behavior in chlorophyll-based DSSCs (Chou, Syu, *et al.*, 2023).

Photovoltaic measurements further confirmed that moderate incorporation of single-layer graphene significantly improved DSSC performance. The highest power conversion efficiency (PCE) of 1.09% was achieved by the TiO_2/single-layer graphene 1.0% v/v photoanode, compared with 0.82% for pure TiO_2. The enhancement in efficiency is attributed to improved electrical conductivity (Amir-Al Zumahi *et al.*, 2021), accelerated electron transport, enhanced light absorption, and suppressed electron–hole recombination provided by the conductive single-layer graphene network (AlSultan *et al.*, 2024). Nevertheless, excessive graphene concentration at 1.5% v/v reduced photovoltaic performance due to graphene agglomeration and increased structural disorder.

Overall, the results demonstrate that single-layer graphene possesses strong potential as an effective conductive material for improving the structural, optical, and photovoltaic properties of TiO_2 photoanodes in environmentally friendly chlorophyll-based DSSCs. Among all investigated samples, the TiO_2/single-layer graphene 1.0% v/v photoanode exhibited the optimum balance between crystallinity, morphology, optical absorption, and charge transport behavior, resulting in the best DSSC performance.

Acknowledgments

Many thanks were delivered to Department of Mechanical Engineering, State University of Malang and Technicians who helped this research.

Author Contributions: Author's contributions and responsibilities – **UHZ**: Funding Acquisition, Project Administration -original draft, and Writing - Review and Editing, Visualization, Methodology, and Investigation. **PT**: Writing – review & Editing, Validation, Methodology, and Investigation. **AA**: Writing – review & Editing, Validation, Methodology, and Investigation, **TATA**: Review & Editing, Validation, and Investigation

Conflicts of Interest: The authors declare no conflict of interest.

References

Agrawal, A., Siddiqui, S. A., Soni, A., & Sharma, G. D. (2022). Advancements, frontiers and analysis of metal oxide semiconductor, dye, electrolyte and counter electrode of dye sensitized solar cell. *Sol. Nergy.*, *233*, 378. https://doi.org/10.1016/j.solener.2022.01.027

Alamu, G. A., Ayanlola, P. S., Babalola, K. K., Adedokun, O., Sanusi, Y. K., & Fajinmi, G. R. (2024). Green synthesis and characterizations of magnetic iron oxide nanoparticles using Moringa oleifera extract for improved performance in dye-sensitized solar cell. *Chemical Physics Impact*, *8*, 100542. https://doi.org/10.1016/J.CHPHI.2024.100542

Alhaji Abubakar, A., Sadiq Abubakar, Y., Mohammed Kimpa, I., Ibrahim Olalonpe, S., & Isah Uthman, K. (2025). Exploring the Impact of Surface Treatments on Electron Transport and Recombination in DSSC Plasmonic Photoanodes: A Systematic Review. *Plasmonics*, 1–25. https://doi.org/10.1007/S11468-025-03011-6/METRICS

AlSultan, H. A., Shafie, S., Hamidon, M. N., Ismail, I., Pandey, S. S., & Ahmad, F. (2024). Advancing dye-sensitized solar cell performance with bifacial illumination: A novel Stack Formation Framework approach. *Optical Materials*, *153*. https://doi.org/10.1016/J.OPTMAT.2024.115535;

Amir-Al Zumahi, S. M., Arobi, N., Mahbubur Rahman, M., Kamal Hossain, M., Ara Jahan Rozy, M., Bashar, M. S., Amri, A., Kabir, H., Abul Hossain, M., & Ahmed, F. (2021). Understanding the optical behaviours and the power conversion efficiency of novel organic dye and nanostructured TiO2 based integrated DSSCs. *Solar Energy*, *225*, 129–147. https://doi.org/10.1016/j.solener.2021.07.024

Amollo, T. A. (2024). Metallic nanoparticles and hybrids of metallic nanoparticles/graphene nanomaterials for enhanced photon harvesting and charge transport in polymer and dye sensitized solar cells. *Heliyon*, *10*(5), e26401. https://doi.org/10.1016/J.HELIYON.2024.E26401

Ashfaq, M., Talreja, N., Singh, N., & Chauhan, D. (2023). 2D-Nanolayer (2D-NL)-Based Hybrid Materials: A Next-Generation Material for Dye-Sensitized Solar Cells. *Electronics (Switzerland)*, *12*(3). https://doi.org/10.3390/ELECTRONICS12030570

Athanasopoulos, E., & Conradie, J. (2024). DFT study of the spectroscopic behaviour of different iron(II)-terpyridine derivatives with application in DSSCs. *Journal of Molecular Graphics and Modelling*, *129*, 108753. https://doi.org/10.1016/J.JMGM.2024.108753

Atilgan, A., & Yildiz, A. (2022). Ni-doped TiO2/TiO2 homojunction photoanodes for efficient dye-sensitized solar cells. *International Journal of Energy Research*, *46*(10), 14558–14569. https://doi.org/10.1002/ER.8175

Ayaz, M., Alatawi, A. S., Hijji, M., Namazi, M. A., & Ershath, M. I. M. (2024). Improving charge transfer properties and solar cell performance by In-doped TiO2 as an efficient photoanode for dye-sensitized solar cells (DSSCs). *Journal of Physics and Chemistry of Solids*, *188*, 111913. https://doi.org/10.1016/J.JPCS.2024.111913

Bandara, T. M. W. J., Gunathilake, S. M. S., Dissanayake, M. A. K. L., Pemasiri, B. M. K., Albinsson, I., & Mellander, B. E. (2024). A review of the development of graphene-incorporated dye-sensitized solar cells. *Ionics 2024 30:11*, *30*(11), 6789–6809. https://doi.org/10.1007/S11581-024-05752-6

Bandara, T. M. W. J., Gunathilake, S. M. S., Gamachchi, G. G. D. M. G., Pemasiri, B. M. K., Ajith DeSilva, L., Dissanayake, M. A. K. L., & Kumara, G. R. A. (2024). Strategic graphene integration in multilayer photoanodes for enhanced quasi-solid-state dye-sensitized solar cells and performance under variable irradiance. *Journal of Applied Electrochemistry*. https://doi.org/10.1007/S10800-024-02204-X

Bhumika, Goyal, R. K., Varshney, M., Sahai, A., Ahemad, F., & Sharma, A. (2026). Next-Generation Oxide-Based Photovoltaics: Role of Carbon Nanotubes, Graphene Derivatives, and Ionic Liquids in Device Engineering. *Journal of Materials Engineering and Performance 2026*, 1–24. https://doi.org/10.1007/S11665-026-14013-8

Bousrez, G., Renier, O., Adranno, B., Smetana, V., & Mudring, A. V. (2021). Ionic Liquid-based Dye-Sensitized Solar Cells - Insights into Electrolyte and Redox Mediator Design. *ACS Sustain. Chem. Eng.*, *9*(24), 8107–8114. https://doi.org/10.1021/acssuschemeng.1c01057/asset/images/large/sc1c01057_0006.jpeg

Chakraborty, A., Lucarelli, G., Xu, J., Skafi, Z., Castro-Hermosa, S., Kaveramma, A. B., Balakrishna, R. G., & Brown, T. M. (2024). Photovoltaics for indoor energy harvesting. *Nano Energy*, *128*. https://doi.org/10.1016/j.nanoen.2024.109932

Chang, Y. C., Tseng, C. A., Lee, C. P., Ann, S. B., Huang, Y. J., Ho, K. C., & Chen, Y. T. (2020). N- and S-codoped graphene hollow nanoballs as an efficient Pt-free electrocatalyst for dye-sensitized solar cells. *Journal of Power Sources*, *449*. https://doi.org/10.1016/j.jpowsour.2019.227470

Chaudhari, A., Kumar, A., Kumar, S., & Kushwaha, S. (2024). Synthesis of TiO2 nanoparticles by green approach: Application as photoanode for dye-sensitized solar cells. *Materials Research Bulletin*, *179*. https://doi.org/10.1016/J.MATERRESBULL.2024.112909

Chou, J. C., Chen, P. F., Yang, P. H., Lai, C. H., Kuo, P. Y., Nien, Y. H., Zhuang, S. W., Syu, R. H., & Huang, Y. H. (2023). Modification of Dye-Sensitized Solar Cells With Sputter-Deposited Titanium Dioxide Blocking Layer for Enhanced Photovoltaic Performance Under Different Illuminations. *IEEE Access*, *11*, 98082–98092. https://doi.org/10.1109/ACCESS.2023.3313558

Chou, J. C., Syu, R. H., Yang, P. H., Kuo, P. Y., Nien, Y. H., Lai, C. H., Chen, P. F., Wu, Y. T., & Zhuang, S. W. (2023). Graphene Quantum Dots as a Co-Sensitizer With Improving Light Absorption for Dye-Sensitized Solar Cells. *IEEE Transactions on Nanotechnology*, *22*, 20–27. https://doi.org/10.1109/TNANO.2023.3235335

Ding, S., Yang, C., Yuan, J., Li, H., Yuan, X., & Li, M. (2023). An overview of the preparation and application of counter electrodes for DSSCs. *RSC Advances*, *13*(18), 12309–12319. https://doi.org/10.1039/D3RA00926B

Dissanayake, M. A. K. L., Senthuran, S., & Senadeera, G. K. R. (2025). Plasmonic enhanced multifunctional composite photoanode for highly efficient dye-sensitized solar cells. *Journal of Solid State Electrochemistry*, *29*(9), 3705–3718. https://doi.org/10.1007/S10008-025-06233-0

Erdogdu, M., Atilgan, A., Erdogdu, Y., & Yildiz, A. (2024). Flavonoid from Hedera helix fruits: A promising new natural sensitizer for DSSCs. *Journal of Photochemistry and Photobiology A: Chemistry*, *448*, 115288. https://doi.org/10.1016/J.JPHOTOCHEM.2023.115288

Hosseinnezhad, M., Ghahari, M., Mobarhan, G., Fathi, M., Palevicius, A., Nutalapati, V., Janusas, G., & Nasiri, S. (2023). New Insights into Improving the Photovoltaic Performance of Dye-Sensitized Solar Cells by Removing Platinum from the Counter Electrode Using a Graphene-MoS2 Composite or Hybrid. *Micromachines*, *14*(12). https://doi.org/10.3390/MI14122161

Hosseinnezhad, M., Gharanjig, K., Ghahari, M., Nasiri, S., & Fathi, M. (2024). Investigation of the use of food waste in renewable energy production: Extraction, fabrication and characterization of natural photosensitizers in DSSCs. *Sustainable Energy Technologies and Assessments*, *72*, 104066. https://doi.org/10.1016/J.SETA.2024.104066

Igman, E., Bayram, O., Mavi, A., Hasar, U. C., & Simsek, O. (2021). Photovoltaic performance of non-covalent functionalized single-layer graphene in dye-sensitized solar cells (DSSCs). *Journal of Materials Science*, *56*(6), 4184–4196. https://doi.org/10.1007/S10853-020-05535-0/FIGURES/9

Iman, R. N., Younas, M., Harrabi, K., & Mekki, A. (2024). Fabrication and characterization of natural dye-sensitized solar cells using an efficient natural sensitizer derived from Laurus nobilis L. *Dyes and Pigments*, *225*. https://doi.org/10.1016/j.dyepig.2024.112057

Irfan, M., Khan, M. I., Ikram-ul-haq, Amami, M., Ahson, R., & Alabbad, E. A. (2022). Alabbad, Effect of Fe ions beam on the structural, optical, photovoltaic properties of TiO2 based dye-sensitized solar cells. *Opt Mater*, *123*, 111794. https://doi.org/10.1016/j.optmat.2021.111794

kavitha, N., Alivelu, M., & Savithajyostna, T. (2024). Synthesis, Theoretical studies, and antibacterial activity of Novel Zn(II) metal complex with salicylaldehyde semicarbazone, and ortho phenylene diamine ligands. *Chemical Physics Impact*, *8*. https://doi.org/10.1016/j.chphi.2024.100602

Konwar, S., Singh, D., Strzałkowski, K., Masri, M. N. Bin, Yahya, M. Z. A., Diantoro, M., Savilov, S. V., & Singh, P. K. (2023). Stable and Efficient Dye-Sensitized Solar Cells and Supercapacitors Developed Using Ionic-Liquid-Doped Biopolymer Electrolytes. *Molecules*, *28*(13), 5099. https://doi.org/10.3390/molecules28135099

Kouhestanian, E., Mozaffari, S. A., Ranjbar, M., & Amoli, H. S. (2020). Enhancing the electron transfer process of TiO2-based DSSC using DC magnetron sputtered ZnO as an efficient alternative for blocking layer. *Organic Electronics*, *86*. https://doi.org/10.1016/j.orgel.2020.105915

Lana, G. M., Bello, I. T., Adedokun, O. M., Adenigba, V. O., Jubu, P. R., Adedokun, O., Sanusi, Y. K., Dhlamini, M. S., & Awodugba, A. O. (2024). One-Dimensional TiO2 Nanocomposite-based Photoanode for Dye-Sensitized solar Cells: A review. *Solar Energy*, *279*, 112850. https://doi.org/10.1016/J.SOLENER.2024.112850

Ma'arifah, A., Sholeha, N., Pujiarti, H., Diantoro, M., Hidayat, A., & Osman, Z. (2025). The effect of RF sputtering power variation on blocking layer TiO2 on the performance of DSSC. *Results in Surfaces and Interfaces*, *18*, 100456. https://doi.org/10.1016/J.RSURFI.2025.100456

Mahalingam, S., Manap, A., Lau, K. S., Omar, A., Chelvanathan, P., Chia, C. H., Amin, N., Mathews, I. J., Afandi, N. F., & Rahim, N. A. (2022). Mixture deposition method for graphene quantum dots-based dye-sensitized solar cell. *Electrochimica Acta*, *404*, 139732. https://doi.org/10.1016/J.ELECTACTA.2021.139732

Mahalingam, S., Manap, A., Rabeya, R., Lau, K. S., Chia, C. H., Abdullah, H., Amin, N., & Chelvanathan, P. (2023a). Electron transport of chemically treated graphene quantum dots-based dye-sensitized solar cells. *Electrochimica Acta*, *439*, 141667. https://doi.org/10.1016/J.ELECTACTA.2022.141667

Mahalingam, S., Manap, A., Rabeya, R., Lau, K. S., Chia, C. H., Abdullah, H., Amin, N., & Chelvanathan, P. (2023b). Electron transport of chemically treated graphene quantum dots-based dye-sensitized solar cells. *Electrochimica Acta*, *439*. https://doi.org/10.1016/j.electacta.2022.141667

Mandal, S., & Kandregula, G. R. (2023). A computational finding on the effect of π-conjugated acceptors in thiophene-linked coumarin dyes for potential suitability in DSSC application. *Journal of Photochemistry and Photobiology A: Chemistry*, *435*, 114300. https://doi.org/10.1016/j.jphotochem.2022.114300

Maurya, I. C., Singh, S., Sharma, S., Kushwaha, S. P. S., Srivastava, P., & Bahadur, L. (2024). Enhanced conversion efficiency enabled with natural dyes extracted from Mirabilis flower and Bixa seed revealing prospects of application of co-sensitized DSSC. *Optik*, *317*, 172072. https://doi.org/10.1016/J.IJLEO.2024.172072

Muchuweni, E., Mombeshora, E. T., Martincigh, B. S., & Nyamori, V. O. (2022). Graphitic carbon nitride-based new-generation solar cells: Critical challenges, recent breakthroughs and future prospects. *Solar Energy*, *239*, 74–87. https://doi.org/10.1016/J.SOLENER.2022.04.039

Muchuweni, E., Mombeshora, E. T., Muiva, C. M., Sathiaraj, T. S., Yildiz, A., & Pugliese, D. (2025). Towards high-performance dye-sensitized solar cells by utilizing reduced graphene oxide-based composites as potential alternatives to conventional electrodes: A review. *Next Materials*, *6*, 100477. https://doi.org/10.1016/J.NXMATE.2024.100477

Muhammad, Sofyan, N., Yuwono, A. H., & Dhaneswara, D. (2025). A review on green synthesis of TiO2 nanoparticles: enhancing DSSC performance and exploring future opportunities. *Materials Science for Energy Technologies*, *8*, 188–199. https://doi.org/10.1016/j.mset.2025.07.001

Prakash, P., & Janarthanan, B. (2023). Review on the progress of light harvesting natural pigments as DSSC sensitizers with high potency. *Inorganic Chemistry Communications*, *152*, 110638. https://doi.org/10.1016/J.INOCHE.2023.110638

Prima, E. C., Rusliani, P. F., Suhendi, E., & Yuliarto, B. (2024). Performance of dye-sensitized solar cells with mixed three natural pigments and reduced graphene oxide as a counter electrode. *Results in Optics*, *14*, 100592. https://doi.org/10.1016/J.RIO.2023.100592

Qamar, S., & Erten Ela, S. (2024). Dye-sensitized solar cells (DSSC): Principles, materials and working mechanism. *Current Opinion in Colloid & Interface Science*, *74*, 101871. https://doi.org/10.1016/J.COCIS.2024.101871

Rahman, S., Haleem, A., Siddiq, M., Hussain, M. K., Qamar, S., Hameed, S., & Waris, M. (2023). Research on dye sensitized solar cells: recent advancement toward the various constituents of dye sensitized solar cells for efficiency enhancement and future prospects. *RSC Advances*, *13*(28), 19508–19529. https://doi.org/10.1039/D3RA00903C

Ramaripa, P. S., Modibane, K. D., Makgopa, K., Seerane, O. A., Maubane-Nkadimeng, M. S., Makhado, E., & Pandey, S. (2023). Influence of phthalocyanine nanowire dye on the performance of titanium dioxide-metal organic framework nanocomposite for dye-sensitized solar cells. *Chemical Engineering Journal Advances*, *14*. https://doi.org/10.1016/J.CEJA.2023.100485

Raveena, J., Chandrapal, R. R., Bakiyaraj, G., Manikandan, V. S., Athitya, S., Archana, J., & Navaneethan, M. (2023). Synergetic effect of 2D/2D Co-SnS2 with reduced graphene oxide heterostructure for Pt-free counter electrode. *Materials Today Communications*, *34*. https://doi.org/10.1016/j.mtcomm.2022.105204

Richhariya, G., Kumar, A., Shukla, A. K., Shukla, K. N., & Chanakaewsomboon, I. (2023). Efficient photosensitive light harvesting dye sensitized solar cell using hibiscus and rhodamine dyes. *Journal of Power Sources*, *572*. https://doi.org/10.1016/j.jpowsour.2023.233112

Richhariya, G., Kumar, A., Shukla, A. K., Shukla, K. N., & Meikap, B. C. (2023). Effect of Different Counter Electrodes on Power Conversion Efficiency of DSSCs. *Journal of Electronic Materials*, *52*(1), 60–71. https://doi.org/10.1007/S11664-022-09973-1

Saadat, F., Alizadeh, A., Roudgar-Amoli, M., & Shariatinia, Z. (2022). Exploring the influence of Zn2SnO4/ZIF-8 nanocomposite photoelectrodes on boosting efficiency of dye sensitized solar cells. *Ceramics International*, *48*(15), 21853–21864. https://doi.org/10.1016/j.ceramint.2022.04.165

Shaikh, R. S., Rajput, R. B., & Kale, R. B. (2024). Inexpensive green synthesis of natural dye-sensitized solar cells with aqueous solution as a Bi2S3 counter electrode. *Next Materials*, *3*, 100051. https://doi.org/10.1016/j.nxmate.2023.100051

Sharma, S. J., Sonigara, K. K., Machhi, H. K., Soni, S. S., & Sekar, N. (2023). Significance of anchoring group design on light harvesting efficiency of dye-sensitized solar cells and non-linear optical response. *Journal of Molecular Structure*, *1294*. https://doi.org/10.1016/j.molstruc.2023.136435

Shikh Zahari, S. M. S. N., Muhamad Tajuddin, N. H., Che Sam, N. F. I., Elzaneen, K. M. H., Puspitasari, P., Weber, C. C., & Mohd Zainon, N. (2023). Iron magnetic nanoparticles coated with different loadings of polyvinylpyrrolidone: Evaluation of magnetic properties and morphology. *Inorganic Chemistry Communications*, *158*. https://doi.org/10.1016/j.inoche.2023.111534

Siddiqui, H., Ali, U., Sahito, I. A., Malik, S. A., Sun, K. C., & Mengal, N. (2024). Comprehensive review of carbon materials as counter electrodes in dye-sensitized solar cells: Efficiency assessment and deposition methods. *Materials Science in Semiconductor Processing*, *172*, 108074. https://doi.org/10.1016/J.MSSP.2023.108074

Teja, A. S., Srivastava, A., Akash Kumar Satrughna, J., Kumar Tiwari, M., Kanwade, A., Lee, H., Ogura, A., & Shirage, P. M. (2023). Synergistic co-sensitization of environment-friendly chlorophyll and anthocyanin-based natural dye-sensitized solar cells: An effective approach towards enhanced efficiency and stability. *Solar Energy*, *261*, 112–124. https://doi.org/10.1016/j.solener.2023.06.004

Tiwari, A., Singh, S., & Srivastava, P. (2024). Exploring the potential of potato starch-capped TiO2 nanoparticles for DSSC photoanodes. *Results in Optics*, *15*. https://doi.org/10.1016/J.RIO.2024.100630

Torres, F. G., & De-la-Torre, G. E. (2022). Green algae as a sustainable source for energy generation and storage technologies. *Sustainable Energy Technologies and Assessments*, *53*, 102658. https://doi.org/10.1016/J.SETA.2022.102658

Trihutomo, P. (2024). Potential of Palm Leaves (Arrenga Pinnata) As Light Wave Absorber and Electron Source in Organic Dye-Sensitized Solar Cells (DSSC). *AIP Conference Proceedings*, *2991*(1). https://doi.org/10.1063/5.0198610/3296816

Trihutomo, P., Marji, Harly, M., Wahyudi, B. A., & Radja, M. B. (2022). The effect of Clathrin protein addition on increasing the number of electrons in organic Dye-Sensitized Solar Cell (DSSC). *EUREKA: Physics and Engineering*, *2022*(2), 15–27. https://doi.org/10.21303/2461-4262.2022.001957

Vibavakumar, S., Nisha, K. D., Archana, J., Navaneethan, M., & Harish, S. (2024). Synergistic effect and enhanced charge transfer in Nb2O5-rGO/TiO2 photoanode for dye-sensitized solar cells. *Sol Energy*, *271*, 112398. https://doi.org/10.1016/j.solener.2024.112398

Xu, H., Zhu, G., & Jin, Z. (2020). Electron migration optimization through nanostructural control of hierarchical Fe3O4 based counter electrodes for high-performance dye-sensitized solar cells. *Journal of Electroanalytical Chemistry*, *869*. https://doi.org/10.1016/j.jelechem.2020.114214

Yan, Y., Zhang, Y., Zhao, Y., Ding, F., Lei, Y., Wang, Y., Zhou, J., & Kang, W. (2025). Review on TiO2 nanostructured photoanode and novel dyes for dye-sensitized solar cells application. *Journal of Materials Science 2025 60:11*, *60*(11), 4975–5005. https://doi.org/10.1007/S10853-025-10734-8

Yeoh, M. E., Chan, K. Y., Wong, H. Y., Low, P. L., How Thien, G. S., Ng, Z. N., Ananda Murthy, H. C., & Balachandran, R. (2023). Hydrothermal duration effect on the self-assembled TiO2 photo-anode for DSSC application. *Optical Materials*, *141*, 113907. https://doi.org/10.1016/J.OPTMAT.2023.113907

Zheng, D., Yang, X., Čuček, L., Wang, J., Ma, T., & Yin, C. (2024). Revolutionizing dye-sensitized solar cells with nanomaterials for enhanced photoelectric performance. *Journal of Cleaner Production*, *464*, 142717. https://doi.org/10.1016/J.JCLEPRO.2024.142717

Znidi, F., Morsy, M., & Nizam Uddin, M. (2024). Recent advances of graphene-based materials in planar perovskite solar cells. *Next Nanotechnology*, *5*, 100061. https://doi.org/10.1016/J.NXNANO.2024.100061